Talanta 237 (2022) 122897

Contents lists available at ScienceDirect

Talanta

journal homepage: www.elsevier.com/locate/talanta

# Spectroscopic ellipsometry methods for brevetoxin detection

Mustafa Oguzhan Caglayan [a,*], Zafer Üstündağ [b], Samet Şahin [a]

[a] Department of Bioengineering, Bilecik Şeyh Edebali University, 11230, Bilecik, Turkey
[b] Department of Chemistry, Kütahya Dumlupınar University, 43100, Kütahya, Turkey

ARTICLE INFO

*Keywords:*
Paralytic shellfish poisoning toxins
Brevetoxin
Seafood
Surface plasmon resonance
Attenuated total internal reflection ellipsometry

ABSTRACT

The spectroscopic ellipsometry (SE), and attenuated internal reflection spectroscopic ellipsometry (TIRE) are promising methods in label-free biosensing applications. An ellipsometer running under surface plasmon resonance (SPR) conditions has unique advantages over other SPR-based methods in terms of sensitivity and real-time/label-free measurement capability. In this study, both SE and TIRE-based brevetoxin B (BTX) sensors were developed using two anti-BTX aptamers reported before. A new aptamer sequence was also derived from these two antiBTX aptamers using predictive modeling tools and an exclusion method. All three antiBTX aptamers' analytical performances were quite competitive in terms of both detecting range and detection limits. However, the selectivity of the previously reported aptamers against analogs of BTX was poor at low detection ranges, especially for okadaic acid. Furthermore, the selectivity of the derived aptamer was lower than its predecessors. The sensors were capable of detecting BTX in the range of 0.05 nM–1600 nM in the TIRE and 0.5 nM–2000 nM in the SE configuration. The detection limits of the sensors were 1.48 nM (1.32 ng/mL) and 0.80 nM (0.72 ng/mL) for SE and TIRE configurations, respectively. Both configurations have been used successfully to detect BTX standards spiked into real fish and shrimp samples.

## 1. Introduction

Brevetoxins (BTXs) are lipophilic polyether neurotoxins produced by a dinoflagellate, *Karenia brevis*, and accumulated in shellfish consuming this alga [1,2]. *K. brevis* and related species naturally occur in the Gulf of Mexico, but since global transportation is inevitable, they result in food safety risks worldwide [3–6]. There are 14 derivatives of BTXs that have already been identified to be produced by *K. brevis* [7,8]. In general, paralytic shellfish poisoning (PSP) occurs due to neurotoxins including okadaic acid (OA), dinophysis toxins (DTX), yessotoxins (YTX), azaspiracides (AZA), pectenotoxins (PTX), cyclic imines, and BTXs synthesized by dinoflagellates [9–12]. These neurotoxins bind to muscle and nerve cells with high affinity, blocking the sodium flow, and preventing the formation and spread of action potentials [13,14]. In the case of acute PSP, symptoms are numbness of the lips and tongue and then the fingers, the loss of control in the arms and legs, and ultimately respiratory distress resulting from paralysis of the chest and abdominal muscles [15]. BTX's have no taste or odor but are also stable against heat and most acids. The most common forms of BTXs are BTXB and BTXC, and these toxins, similar to other PSP toxins, cause neurological poisoning by binding to sodium channels in nerve cells [16]. In addition to threatening the health of humans consuming contaminated seafood with these toxins, the significance of the relationship between BTX poisoning and marine mammals and fish deaths has been reported before in a comprehensive study [17,18]. Although the toxic effects of BTXs have not been proven by inhalation alone, it has been confirmed that they have toxic effects through inhalation along with other biotoxins produced by algae, which indicates that we should consider BTXs as potential bioagents [6,19]. The PSP residue limit adopted by the regulatory authorities to prevent acute poisoning is 0.8 ng PSP toxin/mg seafood [20].

The regulatory testing for these toxins is FDA-approved mouse/rat bioassay. However, both ethical problems and the method's time-consuming nature direct the researchers to the development of different analytical solutions [9,21–23]. A variety of alternative methods include liquid chromatography-tandem mass spectrometry (LC-MS/MS) [11], cell-based bioassays [24–28], receptor binding assays [15,29,30], fluorimetric assays [31–33], enzyme-linked immunosorbent assay (ELISA) [34,35], and electrochemical [36,37]/plasmonic [38,39] immunoassays. However, most of the toxin analysis methods mentioned here are quite laborious and complicated and require some expertise. Although the analytical performance of these analyzes is successful,

* Corresponding author.
*E-mail address:* oguzhan.caglayan@bilecik.edu.tr (M.O. Caglayan).

https://doi.org/10.1016/j.talanta.2021.122897
Received 17 April 2021; Received in revised form 10 August 2021; Accepted 19 September 2021
Available online 4 October 2021

some methods have weaknesses. For example, cell-based analyzes are influenced by the extracellular environment, and the ionic balance in real samples must be adjusted before analysis [40]. Also, specificity levels may exclude the detection of other harmful compounds and potentially underestimate total toxic residue levels. In one comprehensive study, four commercial immunological test kits have evaluated for the detection of PSP toxin in shellfish, and poor analytical results were reported in terms of high false negative and positive results, together with problems in detection limits [41].

Powerful analytical methods such as LC-MS/MS have been developed that provide the appropriate detection limit and range for BTX detection [42,43]. Additionally, ELISA [44,45], radioimmunoassay [46], and electrochemiluminescence-based immunoassays [47] have also been reported. Electrochemical BTX immunosensors based on graphene nanospheres functionalized with gold nanoparticles, dendrimers, or guanine-rich oligonucleotides have been reported [48]. Quartz crystal microbalance (QCM) immunosensors functionalized with graphene have also been used as a different alternative in BTX detection [49–52].

Alternatively, single-stranded DNA or RNA oligonucleotides selected from a random or homologous library, aptamers, have been developed as recognition molecules for PSP toxins [53,54]. Aptamers interact with the target just like the antibody-antigen interaction [55,56]. They are preferred over antibodies that are easily denatured and difficult to manufacture because they have advantages such as stability, low cost, and ease of production [57]. There is a review article on the determination of aquatic toxins using aptamer-based sensors [58]. Some methods, including aptamer-based approaches used in detecting BTX toxins, are listed and compared in Table 1.

Because of the stated advantages of aptamers, for the first time in this study, SE and TIRE performances of two aptamers reported by Eissa et al. ($K_d$ ~ 40 and 100 nM, respectively) were investigated [1]. In ellipsometry, the phase difference (Δ, Delta) and the intensity (Ψ, Psi) of polarized monochromatic light reflected from thin films are measured. These parameters are a function of the refractive index and thickness of the medium in which the light reflected from the surface interacts [61]. Using these parameters obtained from nanofilms on a substrate, surface deposition can be precisely measured. The accuracy of ellipsometric techniques (as low as ±0.001) is highly dependent on the configuration of the ellipsometer used. The Δ is more sensitive to dielectric function change on the substrate and tends to shift to lower degrees when mass accumulation occurs on the substrate due to recognition of the analyte via the recognition element. As is known, SPR is a powerful and label-free technique used for real-time monitoring of biomolecular interactions. Both SPR and ellipsometry use monochromatic and polarized light. In the SPR, plasmon resonance on an ultrathin metal surface is highly sensitive to changes in the dielectric functions of the sensor surface [62,63]. In this study, the analytical performance of the TIRE under SPR conditions and SE methods for BTX detection in seafood samples were evaluated (Fig. 1). An attenuated total internal reflection geometry with a circulating flow cell and an optical coupler similar to the SPR method was used for TIRE experiments to achieve this. Detailed information on surface plasmon resonance and ellipsometry and our previous studies with the specified sensor arrangement can be found in the literature [64–71].

## 2. Materials and methods

### 2.1. Equipment and chemicals

The Optosense 9000 model spectroscopic ellipsometer (Turkey) was used for SE measurements, while a reduced total internal reflection assembly was used for SPR-enhanced measurements using the same ellipsometer. The coupler consists of a BK7 prism (60°, refractive index is 1.58 at 25 °C) and a flow cell to form a Kretschmann geometry [72]. The substrate was a silicon chip since the reflected beam's polarization state is examined in the SE technique, while, in TIRE measurements a gold-coated glass slide was used to obtain an SPR. The glass slide surface to provide the SPR conditions was coated using 3 nm Cr and 50 nm Au film with a high vacuum physical vapor deposition system (NANOVAK, Turkey). Analytical grade chemicals for Au surface blocking agent (6-Mercapto-1-hexanol, MCH), PBS buffer (NaCl 150 mM, $Na_2HPO_4$ 20 mM, EDTA 0.1 mM, Tween 20, 0.005%, pH 7.4), and cleaning solvents (ethanol, isopropanol, etc.) were obtained from local representatives of Sigma-Aldrich or Merck. The glass-slide coating materials (Cr as an adhesive layer, and Au as a plasmon layer) were of coating purity grade of at least 99.95%. Si wafer, the SE substrate, was N-type, polished on one side, and 0.7 mm thick. BTX (Brevetoxin B), OA, saxitoxin (STX), and neo-STX reference solutions were obtained from Sigma-Aldrich's local representative. Unless otherwise stated, all chemical materials were used as purchased and without further purification.

**Table 1**
Comparison of some BTX detection methods reported in the literature.

| Method[a] | Recognition element | Detection limit (LOD) | Range | Description | Reference |
|---|---|---|---|---|---|
| LC-MS/MS | Not applicable | 0.12 pg/mg 13.6 pg/mg tissue | NR | 17 different PSP toxin detection, 12 min detection time | [59] |
| ELISA | Goat anti-BTX antibody | 2.5 pg/mg tissue | 0.2–2 ng/mL | 12 h assay duration | [44] |
| ELISA | Mouse anti-BTX antibody | 5.3 ng/mL | NR | 1.5 h assay duration | [45] |
| ECL | Goat anti-BTX antibody | 50 pg/mL 1 pg/mg tissue | NR | 2 h assay duration | [47] |
| EI | Mouse anti-BTX antibody | 10 pg/mL | 1–10,000 pg/mL | 40 min (approx.) assay duration. Labeled with guanine- graphene nanoribbon complex | [50] |
| QCM | Biotinylated mice anti-BTX antibody | 0.6 pg/mL | 0.01–10 ng/mL | 5 min (approx.) assay duration. Dextran - concanavalin A substitution based immunoassay | [51] |
| EI | HRP labeled mouse anti-BTX antibody | 10 pg/mL | 0.03–8 ng/mL | 15 min (approx.) assay duration. Au nanoparticle and poly (amidoamine) dendrimer | [52] |
| EI | anti-BTX antibody | 1.0 pg/mg | 6–400 pg/mg | 35 min (approx.) assay duration. Screen-printed electrode, toxin immobilized on the SPE via serum albumin fixation. | [60] |
| EIS | anti-BTX aptamer | 106 pg/mL | 0.01–2000 ng/mL | Competitive assay | [1] |
| SE | anti-BTX aptamer | 720 pg/mL in buffer, LOQ ~900 pg/mL in real seafood samples | 0.5 nM–2000 nM | Label-free direct analysis, assay time 90 min plus preparation phase | This paper |
| TIRE | anti-BTX aptamer | 1.32 ng/mL in buffer, LOQ ~1.8 ng/mL in real seafood samples | 0.05 nM–1600 nM | Label-free direct analysis, assay time 90 min plus preparation phase | This paper |

[a] ECL- Electorchemiluminescence, EI- Electrochemical Immunoanalysis, EIS - Electrochemical impedance spectroscopy, SE - Spectroscopic ellipsometry, TIRE - Attenuated internal reflection spectroscopic ellipsometry.

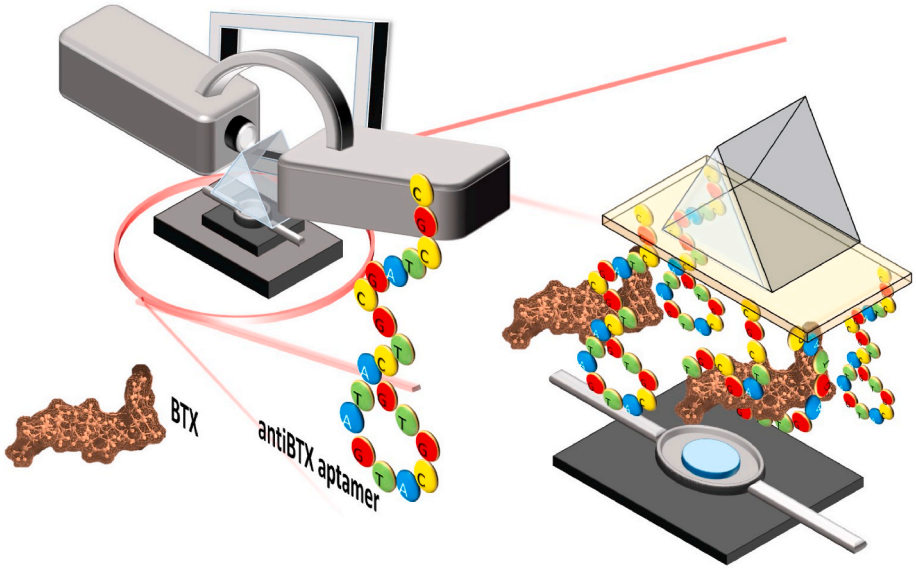


**Fig. 1.** – Schematic diagram of TIRE setup and flow-cell with optical coupler and BTX recognition method.

All substrates were cleaned for 30 min through an oxygen plasma system (RF plasma, Diener, Clairton, USA) before any modification or treatment. All cleaning steps were completed by drying the substrates under a nitrogen atmosphere (99% purity). Milli-Q water (18 MΩ) was used in the preparation of all aqueous solutions. While measuring the upper layers' optical thickness formed on the substrates, the library of dielectric constant-wavelength functions provided with the device was used.

Aptamers were obtained from the local representative of Molbiol (Germany). –SH–$(CH_2)_6$ and –$NH_2$-$(CH_2)_6$ modified aptamers at 5′ termini for surface immobilization were provided. 5'-GTGC GTCC CTGT ACTA GTGA TGAA GCCA AGAG CGCC AACG CTGC CACA CCAA ACCA CCGG-3' (antiBTX1-reported $K_d$ = 42 nM) and 5'-GTTG CCGT CTCC TTAT CCCA CCAC TGCC GACA CCAC CCCC CCGC GAGA GCGA GAGA GCAC T-3' (antiBTX2 – reported $K_d$ = 96 nM) sequences were used as BTX specific aptamer [1]. Another sequence derived from the two specified aptamers was predicted using mfold web server and tested as the antiBTX3 aptamer (http://unafold.rna.albany.edu/). BTX control aptamer (CTRL) (5'-GGTA TTGA GGGT CGCA TCTA GTAG AAAA GTGC TGAG TAGT TTTA CCTG GTAG ATAT GCGA-3') was used as the control

**Table 2**
Aptamers used in this study and their properties[a].

| Sequence (5'-3') and $K_D$ | Secondary structure | Sequence (5'-3') and $K_D$ | Secondary structure |
|---|---|---|---|
| **antiBTX1** $A_{10}$ GTGCGTCCCT$_{20}$ GTACTAGTGA$_{30}$ TGAAGCCAAG$_{40}$ AGCGCCAACG$_{50}$ CTGCCACACC$_{60}$ AAACCACCGG$_{70}$*K*<br>$_d$ 96 nM (R)*K*<br>$_d$ 0.689 μM (F) | 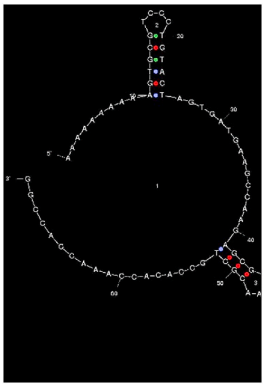 | **antiBTX3**<br>$A_{10}$ CCAAGAGCGC$_{20}$ CAACGCTGCC$_{30}$ ACACCCACCC$_{40}$ CCCCGCGAGA$_{50}$ GCGAGAGAGC$_{60}$*K*<br>$_d$ 1.014 μM (F) | 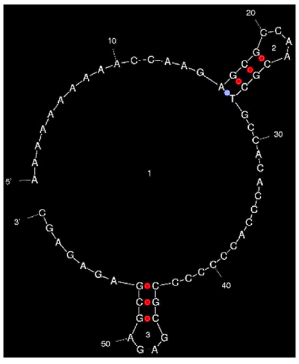 |
| **antiBTX2** $A_{10}$ GTTGCCGTCT$_{20}$ CCTTATCCCA$_{30}$ CCACTGCCGA$_{40}$ CACCACCCCC$_{50}$ CCGCGAGAGC$_{60}$ GAGAGAGCAC$_{70}$ T*K*<br>$_d$ 42 nM (R)*K*<br>$_d$ 0.632 μM (F) | 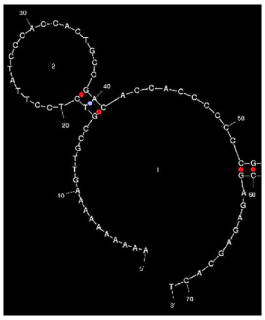 | **CTRL**<br>$A_{10}$ GGTATTGAGG$_{20}$ GTCGCATCTA$_{30}$ GTAGAAAAGT$_{40}$ GCTGAGTAGT$_{50}$ TTTACCTGGT$_{60}$ AGATATGCGA$_{70}$ | 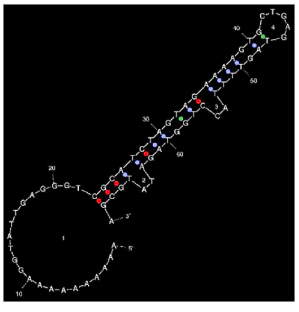 |

[a] Subscripts show base count from 5' termini for convenience. –SH and –$NH_2$ modifications are not represented. $K_d$ values are given as reported (R) and found (F) values where available.

sequence. Sequences, secondary structures, and reported/determined $K_d$ values of aptamers used in the study are given in Table 2.

### 2.2. Preparation of sensor chips

Glass slide surfaces were cleaned by immersing them in a mixture of $H_2SO_4$ and $H_2O_2$ at a 7: 3 by volume for 2 s before coating with Au, then rinsed sequentially using deionized water and ethyl alcohol. The gold coating (50 nm) process was carried out on 3 nm Cr coating by the physical vapor deposition method. Aptamers that carry –SH modification at 5' termini used to prepare aptamer solutions in buffer (0.1, 1.0, and 2.0 μM) were immobilized on Au coated slides, then the optimum aptamer concentration and duration were determined [65,66,70]. After this process, the exposed Au surface was blocked using MCH at a predetermined concentration and time (1 mM and 30 min) [73]. The accumulated layer thickness on the Au-coated was monitored by measuring ellipsometric thickness at each stage (using model data for BK7/Cr/Au/organic layer (n = 1.48)). Thus, the immobilization condition, which gives the maximum surface occupancy and fixed uniformity, has been accepted as the optimum condition. Surface uniformity was determined by comparing the RMS roughness values measured by examining the surface topography using an atomic force microscope (AFM, ParkSystems XE-100, Korea) and performing roughness analysis. A previous study has proven that this approach is sufficient to determine the optimum deposition on the surface during the immobilization phase [68].

For spectroscopic ellipsometry sensor studies, aptamers were immobilized on a modified Si-wafer. The Si-wafer pieces (approx. 1 cm × 1 cm in size) were cleaned by treatment with plasma for 30 min after wet cleaning with nitric acid, hydrogen peroxide, ethyl alcohol, acetone, water, respectively. After cleaning, the –SH terminated surface was obtained on the Si-wafer surface, which was reacted with mercaptopropyl trimethoxysilane (MPTES) prepared in absolute ethyl alcohol at different concentrations. A layer with –COOH functional group was formed using mercaptoundecanoic acid on the surface modified with MPTES. Following the reaction that was performed in the dark overnight for disulfide bond formation, the $NH_2$-modified antiBTX aptamers were then immobilized on the –COOH functionalized surface with the reaction 1-ethyl-3- (3-dimethyl aminopropyl) carbodiimide [65,66]. Optical thickness measurements were made at 500, 550, and 600 nm wavelengths and a 60° and 70° incidence angle for the Au and Si substrate. Then, the thickness was determined by modeling using the device's dielectric function library, based on the Si/$SiO_2$/organic layer (n = 1.48) assumption.

### 2.3. Determination of analytical performances

Ellipsometric sensor response (Δ) was obtained using BTX solution (0.05–1600 nM) in the buffer (ellipsometer set at 60° angle of incidence using 550 nm incident light wavelength). Then the data was used to obtain a calibration curve (from the plateau data after ~ 90 min) as well as to calculate kinetic models. Kinetic parameters were calculated using the real-time sensor response graphs obtained. After dipping the anti-BTX immobilized Si-wafer pieces in BTX solutions (0.5–2000 nM) in phosphate buffer, SE sensor performance was determined by washing (30 min) using only buffer solution after 90 min interaction. Ellipsometric parameters of the dried wafer pieces were then measured using the same equipment directly. The Δ parameter, which changes significantly while molecular recognition occurs, was used to construct the calibration curve.

### 2.4. Seafood sample measurements, selectivity, and accuracy

Test samples of seafood containing BTX were prepared according to the literature [74]. In summary, digestion was performed by weighing 5 g of each fish and shrimp sample obtained from the local market, mixing it with a 1.0% acetic acid aqueous solution for 120 min with a vortex mixer, and then heating it in a water bath at 85 °C for 10 min. Then the samples were allowed to cool to room temperature using a vortex-shaker for 60 s at intervals of every 5 min. The homogenized samples were then centrifuged at 7000 rpm for 10 min. The supernatant obtained was evaporated and taken into buffer solution and used in all real sample measurements. With the addition method, BTX solutions were prepared so that the final BTX concentration was 10, 100, and 1000 nM and added into the real samples. Then, BTX in the digested real samples kept in the fridge for 1 day was extracted from 1 mL of real sample, this time using 5 mL of methanol containing 1.0% acetic acid. The extraction process was continued ultrasonically for 30 min in an ice bath, and then the liquid phase taken from the centrifuged sample was used in BTX analysis. To determine the selectivity of antiBTX aptamers, neo-STX (NEO), STX, and OA were added to 10 and 1000 nM BTX solution at a final concentration of 1000 nM. Thus, 1 and 100-fold interferent concentrations were obtained per extracted BTX, and selectivity was determined.

## 3. Results and discussion

### 3.1. Development of antiBTX3 aptamer

The secondary structure of aptamers describes which nucleotides form Watson-Crick base pairs and which ones are in loops [75]. There are some available resources used in determining this secondary structure. It has been reported that among these resources, the algorithm that can make the predictions/calculations in the best way is presented by "mfold" [76]. Considering aptamers' basic properties in this study, a new aptamer has been proposed using the crawling method [77]. The previously reported antiBTX1 and antiBTX2 aptamers, both of which have two hairpin loops, were used for this purpose. Two stem-loop parts of antiBTX1, i.e. **$A_{10}$GTGC$G_{15}$ -TCCC – $T_{20}$GTAC$T_{25}$** in between $G_{15}$-$T_{20}$ (∂G +3.30 kcal/mol), and **$A_{41}$GCG-C$_{45}$CAA-CG$_{50}$CT** in between $G_{44}$-$C_{49}$ (∂G +2.50 kcal/mol), are the possible interactive parts of the aptamer for BTX recognition. Here, for convenience, base counts beginning from the 5′ termini of the aptamer are shown with a subscript.

Similarly, **$G_{17}$TC-$T_{20}$ CCTTA$_{25}$TCCCA$_{30}$ CCACT$_{35}$GCC- GA$_{40}$ C** in between $C_{19}$-$G_{39}$ (∂G +4.40 kcal/mol) and **C$_{52}$GC-G$_{55}$AGA-GC$_{60}$G** in between $C_{54}$-$G_{59}$ (∂G +1.40 kcal/mol) stem-loop parts of antiBTX2 are possibly involving in the BTX interaction. In general, the loop region in the aptamer's secondary structure tends to bind more to the target than the body region. Therefore, isolating the loop region to obtain short functional aptamer parts without disrupting the main structure could be very useful. This process is called the crawling technique. The functional and smaller part of the aptamer is obtained by gradually removing bases from both ends, with comparing modeling results of secondary structures in each step [77] (Table S1).

Both aptamers used for BTX in this study also have two hairpin loops. Therefore, it has been estimated that the hairpin loops of **$A_{41}$GCG-C$_{45}$CAA-CG$_{50}$CT** between $G_{44}$-$C_{49}$, and **$A_{10}$GTGC$G_{15}$ -TCCC – $T_{20}$GTAC$T_{25}$** between $G_{15}$-$T_{20}$ are interacting structures with BTX in antiBTX1 aptamer. Similarly, both hairpin loops of **$G_{17}$TC-$T_{20}$ CCTTA$_{25}$TCCCA$_{30}$ CCACT$_{35}$GCC- GA$_{40}$ C** between $C_{19}$-$G_{39}$, and **C$_{52}$GC-G$_{55}$AGA-GC$_{60}$G** between $C_{54}$-$G_{59}$ are possibly the active regions of antiBTX2 aptamer. In the antiBTX1 aptamer, the first loop is close to the forward primers. Generally, the aptamer is less likely to be bound by bases close to the primary site. Therefore, the second hairpin loop in antiBTX1 was considered to be used in the new aptamer design. Besides, molecular mechanics 2 (MM2) modeling was performed using the $C_{19}$-$G_{39}$ aptamer fragment in the antiBTX2 aptamer.

Taking into consideration that solvent interaction was not included in the modeling, the distance between C atom number 250 and O atom number 417 in the structure estimation was calculated as 1.6 nm. This value was considered a measure of the diameter of the loop. The dimensions of the BTX molecule were also calculated as approximately 2.7 nm × 0.6 nm. On the other hand, due to the physical width of the

$C_{19}$-$G_{39}$ loop in the antiBTX2 aptamer and its deviation from the optimal energy as seen in the dot-plot, and the higher this deviation compared to the optimal energy in the stem region, this loop has not been included in the new aptamer design. Using these arbitrary but relatively structural analysis-based predictions, the $A_{41}$GCG-$C_{45}$CAA-$CG_{50}$CT sequence between $G_{44}$-$C_{49}$ in antiBTX1, and $C_{52}$GC-$G_{55}$AGA-$GC_{60}$G sequence between $C_{54}$-$G_{59}$ in antiBTX2 were selected and used in the new aptamer design. In the antiBTX2 aptamer, new secondary structures were calculated by removing the bases two by two from each end with the crawling method (Table S2). For convenience, the crawling steps were shown in detail for antiBTX2, while for antiBTX1 they were shown as the final step. Although there were fluctuations in the energy distribution and secondary structure in the intermediate steps compared to the original aptamer, the final fragments obtained showed small deviations in energy distribution and structure compared to the original. Fragments from both aptamers were combined to get the new aptamer sequence (Table 2).

### 3.2. Optimization of aptamer immobilization conditions

Since all antiBTX aptamers used in the present study are approximately 60 bases in size, the most appropriate aptamer immobilization condition was determined using only the antiBTX1 aptamer. Ellipsometric and electrochemical-based aptasensors for various target molecules have been developed and reported by our group [64–67]. In these studies, it was evaluated that the most important factor in the immobilization of aptamers on the Au or Si surface (although the base type distribution also has some effect) is the base number. It was determined that the binding response reached the plateau in ~90 min by examining the immobilization time simultaneously for the SH-modified aptamers. Moreover, 120 min was thought to be more appropriate and sufficient as the duration of the immobilization process since it was performed at room temperature. The RMS roughness values were determined as 0.3 ± 0.04 nm for the blank Au surface and 2.09 ± 0.25 nm (after 120 min immobilization time) for the Au-coated slide immobilized with 1 μM antiBTX1 aptamer (Figure S1). The ellipsometric thickness of the upper layer formed after 120 min was 3.21 ± 0.37 nm. This thickness increased to 3.92 ± 0.33 nm after an additional 2 h. The ellipsometric thickness did not increase significantly after a certain time was interpreted as the immobilization time at the end of 120 min was sufficient. This result is similar to published values in our previous studies depending on the substrate and aptamer size used [73].

In Si-wafer immobilization, the RMS roughness was 0.7 ± 0.1 nm for the empty wafer, while the RMS roughness for the 1 μM antiBTX1 aptamer immobilized Si-wafer was 1.54 ± 0.08 nm (after 120 min). With increasing the concentration to 2 μM antiBTX1, at the end of 120 min, RMS roughness increased to 2.21 ± 0.47, while a slight increase was observed in thickness values. After 120 min, the thickness of the layer on the Si-wafer reached 4.21 ± 0.87 nm, and a non-uniform thickness of 5.05 ± 1.21 nm was obtained for the 240th min. As a result of these measurements, which are considered as an indicator of physical agglomeration, it was decided that the most appropriate immobilization duration was 120 min, and the concentration of the aptamer was 1 μM. It should not be forgotten that the values stated here are not a measure of the full surface coverage, but rather experimentally standard and appropriate values. Surface coverage and self-assembling monolayers are another research area and similar studies have been done by our group before, but they are not covered in this study [68].

### 3.3. TIRE sensor response and calibration curves

The real-time sensor response of the aptamers used in this study was obtained using 0.05 nM–1600 nM BTX. The data (at 30 s interval) acquired by TIRE was used to calculate the kinetics of the interaction between the antiBTX aptamer and BTX at room temperature. As seen in Fig. 2, the sensor signal increase after BTX injection is proportional to the initial BTX concentration. Since the experiments were carried out at room temperature, the time to equilibrium for the BTX-antiBTX1 interaction was approximately 90 min. One of the main reasons for both may be that the size of the BTX molecule (895 g/mol), and slow adsorption to the sensor chip due to its lipophilic nature.

Moreover, the fact that no additional processes were made to increase the surface area during the ligand's immobilization to the sensor chip and the concentration of both analyte and ligand is very low also affected the interaction rate. After 90 min (deviation of 1–2 min due to the operator), the elution solution in the buffer was injected in the whole set of experiments, and the disassociation trend was followed up to 180 min. The signal revealed by the maximum interfering substance (OA,

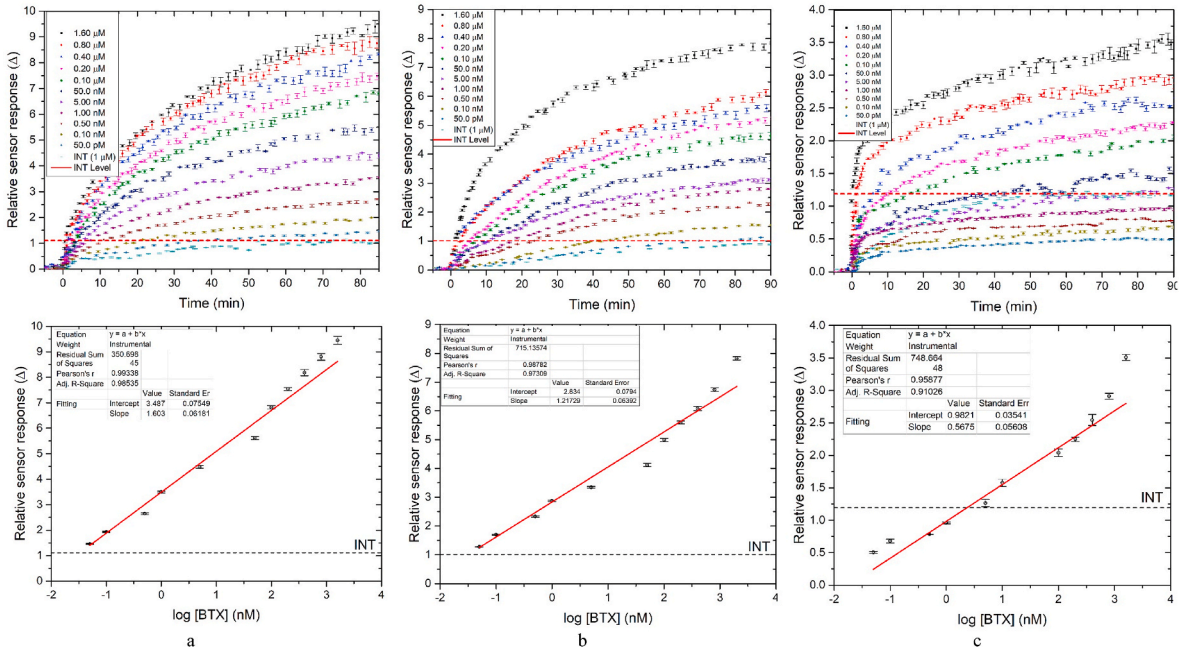


**Fig. 2.** Sensor responses and calibration curves for antiBTX1 (a), antiBTX2 (b), and antiBTX3 (c) in the TIRE system.

henceforth referred to as INT) at 1.0 μM concentration is given in the same graph. Sensor responses were given in terms of the mean and standard deviation of 3 analyzes and are reported by reducing the number of data presented in the graph due to the frequent plot points. In the antiBTX2 aptamer, it was observed that the sensor response at 1600 nM BTX concentration was in a trend that quickly filled the empty aptamer receptors on the surface compared to antiBTX1 and the analyte concentration was high enough to ensure saturation. However, where the BTX concentration was slightly lower (i.e. 800 nM), the binding trend between BTX and the antiBTX2 aptamer was obtained similar to the behavior of the antiBTX1 aptamer. The maximum response of the antiBTX2 sensor was higher than antiBTX3 but lower than antiBTX1 (~1°). The experiments with the antiBTX3 aptamer were noisier than the other two aptamer results, considering the width of the error bars given in σ. However, it is also seen that antiBTX3 accumulates faster on the sensor surface during the first 20–40 min compared to both antiBTX1 and antiBTX2 and there are small oscillations in the sensor response curves. Although the sensor signal was received at low BTX concentrations, it can be said that the selectivity of the antiBTX3 aptamer was low due to the INT signal being 1.19°. Signals obtained with BTX concentration less than 5 nM gave a sensor result below the INT signal.

Approximately 90 min after injection of 0.05–1600 nM BTX, the values obtained as the mean and standard deviation of 10 data taken from the maximum region of the binding curves approaching equilibrium were used for obtaining sensor calibration curves (Fig. 2). The LOD (3σ = 0.155) for AntiBTX1 was calculated as 0.01 nM. However, considering the mean INT signal, the LOD (3σ) for BTX (taking the mean signal 1σ = 1.11 Δ) was calculated as 0.80 nM. Within the 95% confidence limit, the quantization limit (LOQ) corresponds to 3x LOD. Within the 95% confidence limit, the quantification limit (LOQ) was 2.4 nM for antiBTX1. LOD and LOQ values were calculated for other aptamers and analytical performances of antiBTX aptamers in BTX detection performed using the TIRE method are given in Table 3.

The high detection limit of the antiBTX3 aptamer (1.14 μM BTX) corresponds to a detection limit of 104 times higher compared to the other two aptamers. For two aptamers with similar analytical performances, the LOD levels of 0.032 nM (0.029 ng/mL) and 0.8 nM (0.716 ng/mL) were quite satisfactory. In addition, sensors capable of operating in the range of 0.05 nM (0.045 ng/mL) - 1600 nM (1432 ng/mL) provided sufficient analytical performance for the determination of BTX.

### 3.4. SE sensor response and calibration curves

Sensor responses in the SE configuration of the aptamers were obtained in the presence of 5000 nM–0.5 nM BTX. The sensor responses (mean and ± σ of 4 repetitions) obtained by using monochromatic light at 400–1700 nm wavelength at 70° light incident angle are given in Fig. 3. The aptamer carrying only sensor surface was denoted as bare surface. The ellipsometric sensors' behavior is that the wavelength-Δ curves obtained from the substrate shift towards lower degrees as the accumulation on the surface.

As can be seen, when the signal obtained from the bare sensor chip was in the range of 170–180°, after BTX binding to the surface and thus organic material accumulation, this signal shifted to the range of 155–160° for 5000 nM BTX by following approximately the same trend. Moreover, the wavelength dependence of values in the antiBTX3 sensor was more linear at high BTX concentrations. It was observed that the result obtained for 0.5 nM BTX coincided with the result obtained from the bare chip and did not differ significantly. Sensor responses were reported by taking relative responses to the bare chip signal (Figure S2). Differential sensor response decreased almost parallel for all concentrations, with a near-zero slope (~$10^{-4}$) between 400 and 1700 nm. However, the Δ value measured from different wavelengths was found to be quite noisy, despite the resolution of the instrument ~0.001° and repeatability ~0.005°. Although all measurements are made in the room where an air conditioner is used for temperature and humidity control, thermal drift and/or an additional absorbed water vapor layer during the measurement may be the reason for this shift in Δ value. However, temperature control and humidity control measures to eliminate this shift are unfortunately not cost-effective.

For this reason, while creating calibration curves from sensor responses, the statistical evaluation using a one-sample *t*-test was made using all of the Δ values obtained for 400–1700 nm for each BTX concentration. The upper and lower limits were obtained with the mean value at a 95% confidence interval, and the sensor calibration graph was created using these data. The INT and noise levels are shown on the same graph (Fig. 3).

For antiBTX1, the signal received from the sensor (Δ = 0.417) was above the noise level (Δ = 0.269) for 0.5 nM BTX, although the signal obtained for INT (Δ = 0.858) was higher than the signal obtained from the lowest BTX concentration. The INT signal for antiBTX3 was high, but the highest INT signal was obtained in the interaction between antiBTX2 and INT and was 1.264 Δ. Therefore, after the calibration curves were obtained, two different baseline values were used to calculate LOD values. For example, the calibration curve for antiBTX1 fit the line Δ = 3.023(log[BTX])+2.059 with a 0.95 coefficient of determination. The LOD obtained by taking the S/N ratio 3 (3σ = 0.807) from this calibration curve was 0.39 nM. However, because the interference signal obtained for INT was higher than the BTX signal, the BTX limit measured using this sensor was determined as 1.48 nM, taking 3INT = 2.574 at a 95% confidence interval. The limit of quantification was calculated as 4.44 nM BTX using the general approach, 3x LOD. Similarly, LOD and LOQ values calculated for all aptamers are given in Table 3. For antiBTX2, the LOD (3σ = 0.821) was 0.90 nM, and the measurable BTX limit was determined as 10.6 nM, taking 3INT = 3.792 at 95% confidence interval. The limit of quantification was calculated as 31.8 nM BTX using a similar manner. For antiBTX3, the LOD (3σ = 1.194) was 0.82 nM, the measurable BTX limit (3INT = 6.423) was 142.5 nM and the quantization limit was calculated as 427.5 nM BTX.

The 0.39 nM LOD value obtained for antiBTX was 3 times lower than other SE-based antiBTX aptasensors in this study (Table 3). Also, the calibration line slope, a measure of precision, was obtained higher for the antiBTX1 aptamer (~10% better). However, in all SE analyzes, the INT molecule (1000 nM) revealed a signal Δ~1° after washing, possibly due to physical accumulation, and higher than the signal obtained from the lowest BTX concentration. Especially for antiBTX3 aptamer, this non-specific binding was relatively high and caused the LOD to increase to 143 nM. However, for both aptamers (antiBTX1 and antiBTX2)

**Table 3**
Comparison of the analytical performance of antiBTX aptamers in BTX detection by TIRE and SE method.[a]

| | Aptamer | Slope | Intercept | NL (σ, Δ) | $LOD_{NL}$ (nM) | INT (Δ) | $LOD_{INT}$ (nM) | $LOQ_{INT}$ (nM) |
|---|---|---|---|---|---|---|---|---|
| TIRE | antiBTX1 | 1.603 | 3.487 | 0.155 | 0.010 | 1.11 | 0.80 | 2.40 |
| | antiBTX2 | 1.217 | 2.834 | 0.074 | 0.007 | 1.01 | 0.032 | 0.095 |
| | antiBTX3 | 0.982 | 0.568 | 0.153 | 0.774 | 1.19 | 1140 | 3420 |
| SE | antiBTX1 | 3.023 | 2.059 | 0.269 | 0.390 | 0.86 | 1.48 | 4.44 |
| | antiBTX2 | 2.764 | 0.954 | 0.274 | 0.900 | 1.26 | 10.6 | 31.8 |
| | antiBTX3 | 2.334 | 1.396 | 0.398 | 0.820 | 2.14 | 143 | 428 |

[a] Slope and Intercept: The slope and the intercept of the calibration line. NL: Noise level, Δ. $LOD_{NL}$: Limit of detection calculated using NL, nM. INT: Interferent signal level, Δ. $LOD_{INT}$: Limit of detection calculated using INT, nM. LOQ: Limit of quantification, nM.

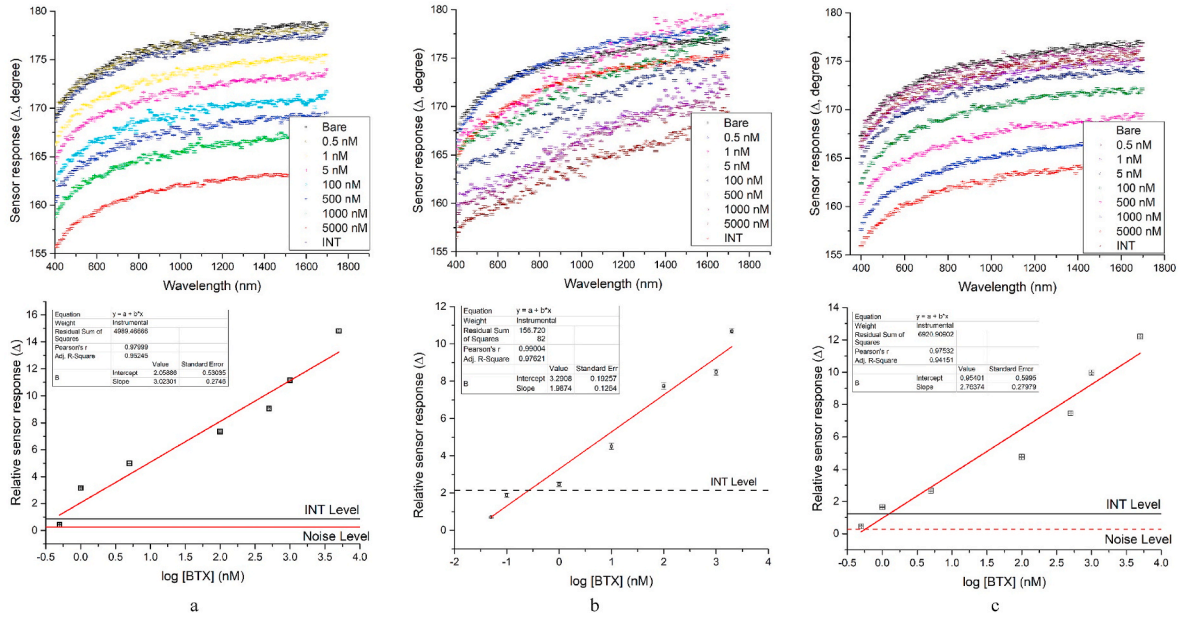


**Fig. 3.** – Sensor responses and calibration curves for antiBTX1 (a), antiBTX2 (b), and antiBTX3 (c) in the SE system.

reported in the literature, the LOD value calculated by considering the interference was 1.48 nM and 10.6 nM, respectively (Signal/INT level = 3). The LOQ for these two sensors was calculated as 4.4 and 32 nM BTX, respectively.

### 3.5. Kinetic parameters

Using the data obtained from TIRE sensor responses, the kinetic behavior of antiBTX1-antiBTX3 aptamers for 1600 nM–005 nM BTX was investigated. For this purpose, $k_{on}$, $k_{off}$, and $K_d$ values were calculated by modeling, from binding curves for one aptamer (See Section S.4).

For antiBTX1, $k_{on}$ value was $1.6 \times 10^4$ $M^{-1}min^{-1}$, the $k_{off}$ value was 0.011 $min^{-1}$ and the calculated $K_d$ value was 0.69 μM. As a result of the calculations made for antiBTX2, it was determined that the $k_{on}$, $k_{off}$, and $K_d$ values were $1.7 \times 10^4$ $M^{-1}min^{-1}$, 0.011 $min^{-1}$, and 0.63 μM, respectively. On the other hand, for the aptamer developed in silico with the exclusion method, it was determined that $k_{on}$, $k_{off}$, and $K_d$ values were $3.2 \times 10^4$ $M^{-1}min^{-1}$, 0.033 $min^{-1}$, and 1.01 μM, respectively.

The kinetic results obtained from the aptamers from the literature were close to each other. There is no significant difference between the $k_{on}$ and $k_{off}$ constants and the equilibrium dissociation constant for both aptamers. On the other hand, for the antiBTX3 aptamer, the $k_{on}$ was found to be twice as high while the $k_{off}$ was found to be 3 times higher. In addition, the equilibrium dissociation constant was obtained twice as high.

It was observed that the calculation of kinetic constants was dependent on the analyte concentration. Kinetic modeling resulted in a lower error for higher concentrations (1600-100 nM) and lower concentrations (<100 nM). However, it was deemed more appropriate to give modeling results using all data. On the other hand, calculated $K_d$ values were slightly lower than the reported $K_d$ values. This may be because the reported $K_d$ value was measured in solution with a fluorescent label, but in our study, experiments were performed with an aptamer immobilized on the surface.

### 3.6. Repeatability, reliability, and real sample measurements

The specificity of the aptasensor probes has been tested using the CTRL aptamer. For this purpose, sensor response was examined using sensor chips with CTRL aptamer interacted with 1000 nM BTX (in PBS). In CTRL/TIRE system, it was observed that BTX caused a change of $0.732 \pm 0.092°\Delta$ at 1000 nM concentration at the end of 90 min, while this concentration caused a change of $0.425 \pm 0.124°\Delta$ in the CTRL/SE system. Although both of these values were slightly higher than the standard deviation (i.e., the noise level) of the lowest BTX concentration's sensor response, they remained well below the specified detection limits (LOD). This resulted from the DNA sequence composed of random sequences and lacking regions suitable for BTX binding [78].

To evaluate the selectivity of the proposed sensor chips, OA structurally similar to BTX, saxitoxin (STX), and STX-like neosaxitoxin (NEO) certified reference solutions were also used as interfering components [73]. The effect of the selected interfering agents on the sensor response at different concentrations is given in Table 4. When 100-fold interferent was added, the signal received for NEO and STX remained below 10% for the equivalent signal for both antiBTX1 and antiBTX2, but it reached 24% for antiBTX3. On the other hand, OA interfered with BTX for all aptamer groups, causing a positive bias of around 15% for the antiBTX1 and antiBTX2 aptamers, and a 46% positive bias against antiBTX3 aptamer. Moreover, the interferent effect slightly decreased with BTX when the interferent ratio was 1/1. For antiBTX1 and antiBTX2 aptamer, the positive bias due to the interferent effect decreased to around 5% for NEO and STX, while it was ~10% for OA. The positive bias for antiBTX3 was around ~10% for NEO and STX, while it was 20.3% when OA was used.

Interestingly, for SE, interference effects caused lesser bias than the TIRE in the sensor signal. In particular, the SE sensor's low sensitivity may have caused the interferent effect to be less felt. On the other hand, it can be said that OA, NEO, and STX molecules, which are bound by non-specific interactions, move away from the surface in the washing process in the SE sensor. But in the circulating TIRE system, they were re-bound to the surface with a certain kinetic balance even if they moved away from the surface. For antiBTX1 and antiBTX2, the positive bias caused by STX and NEO interferents at 1- and 100-times concentrations in the sensor signal was around 5%, while OA caused a deviation up to 20% at low concentrations.

The TIRE and SE methods' precision and accuracy were evaluated using 10 nM and 1000 nM BTX solutions. Five independent sensor chip series were used for intra-day measurements. Five independent series of chips were tested on five consecutive days for inter-day measurements.

The precision and accuracy of both methods are given in Table 5. The accuracy of the methods for intra-day measurements was between −9.58% and +7.20% for antiBTX1 and antiBTX2 aptamer. Inter-days

**Table 4**
The bias observed in the sensor signal (given as %Δ) resulted from the interaction of interferents similar to BTX with the sensor chip at a concentration of 100 times BTX.

| Aptamer | BTX added | INT | INT (nM) | Bias TIRE | Calculated BTX (nM) | Bias SE | Calculated BTX (nM) |
|---|---|---|---|---|---|---|---|
| antiBTX1 | 10 | OA | 1000 | 17.4 | 35.8 | 13.5 | 16.8 |
| | 10 | NEO | 1000 | 7.1 | 16.8 | 5.1 | 12.2 |
| | 10 | STX | 1000 | 5.8 | 15.3 | 4.0 | 11.7 |
| antiBTX2 | 10 | OA | 1000 | 15.0 | 31.4 | 20.4 | 18.8 |
| | 10 | NEO | 1000 | 7.3 | 17.7 | 10.1 | 13.7 |
| | 10 | STX | 1000 | 5.5 | 15.4 | 5.2 | 11.7 |
| antiBTX3 | 10 | OA | 1000 | 46.0 | 53.3 | 34.4 | 35.5 |
| | 10 | NEO | 1000 | 24.5 | 27.4 | 18.0 | 19.4 |
| | 10 | STX | 1000 | 15.1 | 21.3 | 11.6 | 15.3 |
| antiBTX1 | 1000 | OA | 1000 | 10.7 | 3580 | 6.1 | 1686 |
| | 1000 | NEO | 1000 | 4.4 | 1681 | 2.3 | 1216 |
| | 1000 | STX | 1000 | 3.6 | 1529 | 1.8 | 1167 |
| antiBTX2 | 1000 | OA | 1000 | 9.3 | 3147 | 8.2 | 1880 |
| | 1000 | NEO | 1000 | 4.6 | 1768 | 4.0 | 1366 |
| | 1000 | STX | 1000 | 3.5 | 1539 | 2.1 | 1174 |
| antiBTX3 | 1000 | OA | 1000 | 20.3 | 5334 | 15.3 | 3551 |
| | 1000 | NEO | 1000 | 11.1 | 2495 | 8.0 | 1940 |
| | 1000 | STX | 1000 | 7.0 | 1780 | 5.1 | 1531 |

**Table 5**
The precision and accuracy results of the proposed methods (mean ± σ).

| Aptamer | Method | Added BTX (nM) | Intra-day | | | Inter-days[a] | | |
|---|---|---|---|---|---|---|---|---|
| | | | Found BTX (nM) | Precision % | Accuracy% | Found BTX (nM) | Precision % | Accuracy % |
| antiBTX1 | TIRE | 10 | 9.05 ± 0.47 | 5.19 | −9.51 | 9.89 ± 0.95 | 9.65 | −1.14 |
| | | 1000 | 1023 ± 34 | 3.30 | 2.30 | 1005 ± 43 | 4.31 | 0.51 |
| | SE | 10 | 10.41 ± 0.21 | 1.97 | −4.13 | 9.77 ± 0.40 | 4.14 | −2.29 |
| | | 1000 | 992 ± 21 | 2.07 | −0.76 | 1020 ± 7 | 0.71 | +2.02 |
| antiBTX2 | TIRE | 10 | 10.72 ± 0.37 | 3.46 | 7.20 | 10.27 ± 1.11 | 10.77 | 2.74 |
| | | 1000 | 1015 ± 33 | 3.28 | 1.49 | 1031 ± 63 | 6.12 | 3.05 |
| | SE | 10 | 9.04 ± 0.63 | 6.94 | −9.58 | 11.08 ± 0.38 | 3.51 | 10.82 |
| | | 1000 | 1050 ± 26 | 2.47 | 5.08 | 976 ± 42 | 4.33 | −2.3 |
| antiBTX3 | TIRE | 100 | 127.8 ± 21.8 | 17.1 | 27.8 | 118.3 ± 33.2 | 28.1 | 18.3 |
| | | 1000 | 999 ± 322 | 32.2 | −0.08 | 1163 ± 234 | 20.1 | 16.26 |
| | SE | 10 | 9.43 ± 1.84 | 19.53 | −5.73 | 11.27 ± 1.96 | 17.44 | +12.7 |
| | | 1000 | 1082 ± 30 | 2.8 | +8.29 | 1051 ± 84 | 8.02 | +5.17 |

[a] Five consecutive days.

accuracies were between −2.30% and +10.8%. The maximum deviations for antiBTX3, both intra-day and inter-days, were +10.8% and −9.6%, and the method accuracy for antiBTX1 and antiBTX2 can be said to be ±10%. On the other hand, for antiBTX3, the situation was somewhat different and the intra-day accuracy was determined between +27.8 and −5.7%, while the inter-day accuracy was always between 5.17% and 18.3%.

In addition, the intra-day precision of the methods was again between 1.97% and 6.94% for antiBTX1 and antiBTX2 aptamers, while the inter-day precision was between 0.71% and 10.8%. However, the intra-

**Table 6**
Analytical recovery data from sea products of the proposed sensors (Experiments were repeated 3 times and given as the results' average results. All concentrations are in nM).

| | Sample | Added | Found by TIRE | Error (%) | Added | Found by SE | Error (%) |
|---|---|---|---|---|---|---|---|
| antiBTX1 | *Salmo trutta* | 1.0 | 0.94 ± 0.03 | −5.2 | 2.00 | 2.07 ± 0.25 | 3.7 |
| | | 100.0 | 100.4 ± 2.1 | 0.4 | 100.0 | 99.1 ± 1.8 | −0.9 |
| | | 1000 | 1036 ± 27 | 3.6 | 1000 | 991 ± 8 | −0.9 |
| | *Pandalus borealis* | 1.00 | 1.07 ± 0.01 | 6.9 | 2.00 | 1.87 ± 0.14 | −6.5 |
| | | 100.0 | 98.0 ± 1.27 | −2.0 | 100.0 | 101.1 ± 2.9 | 1.1 |
| | | 1000 | 1007 ± 25 | 0.7 | 1000 | 1020 ± 14 | 2.1 |
| antiBTX2 | *Salmo trutta* | 1.00 | 0.98 ± 0.01 | −1.9 | 1.00 | 0.99 ± 0.17 | −0.1 |
| | | 100.0 | 99.5 ± 1.9 | −0.5 | 100.0 | 98.5 ± 2.8 | −1.5 |
| | | 1000 | 1021 ± 15 | 2.1 | 1000 | 1005 ± 18 | 0.6 |
| | *Pandalus borealis* | 1.00 | 1.03 ± 0.01 | 3.5 | 1.00 | 1.07 ± 0.14 | 7.1 |
| | | 100.0 | 102.8 ± 1.7 | 2.8 | 100.0 | 101.8 ± 1.9 | 1.8 |
| | | 1000 | 987 ± 8 | −1.3 | 1000 | 1009 ± 19 | 0.9 |
| antiBTX3 | *Salmo trutta* | 100.0 | NA | NA | 100.0 | 98.1 ± 6.0 | −1.9 |
| | | 1000 | 922 ± 69 | −7.8 | 1000 | 984 ± 19 | −1.5 |
| | | 2000 | 2110 ± 162 | 5.5 | 2000 | 1869 ± 64 | −6.5 |
| | *Pandalus borealis* | 100.0 | NA | NA | 100.0 | 102.2 ± 7.1 | 2.2 |
| | | 1000 | 1090 ± 39 | 9.0 | 1000 | 1070 ± 42 | 7.0 |
| | | 2000 | 1787 ± 101 | −10.7 | 2000 | 1951 ± 85 | −2.4 |

day and inter-day precision for antiBTX3 were 32.2% and 28.1%, respectively. According to the results stated, it can be said that the precision remains within ±10% for antiBTX1 and antiBTX2, whether in SE or TIRE configuration. On the other hand, the SE method's accuracy and precision results intra-day and inter-day were found to be better than the TIRE method.

Analytical performances of TIRE and SE aptasensors were also evaluated using real samples (Table 6). Seafood samples with BTX added were tested using the procedures given above. Fish (*Salmo trutta*) and shrimp (*Pandalus borealis*) samples were purchased from the local market. Theoretically, products claimed to be sourced from local marine farms should have no BTX residue. For the TIRE method, BTX was added to the actual samples, ensuring that the final extracted amount for the assay was 1.00, 100.0, and 1000.0 nM BTX in the buffer solution. However, since the LOD value of the antiBTX3 aptamer and TIRE combination is 143 nM, only real samples with BTX addition of 1000 and 2000 nM were used for the antiBTX3/TIRE combination. For the antiBTX1 and antiBTX2 aptamers, the measurement deviations from the added amount in the fish sample were between −5.2 and + 3.6% (94.8% and 103.6% as recovery), while the deviations for the shrimp samples were between −2.0 and + 6.9% (98%–106.9% as recovery). These results are very satisfactory in terms of actual sample applicability. However, for the antiBTX3 aptamer, the results were somewhat disappointing. While a deviation of −7.8% and +5.5% was obtained for fish at high concentrations (92.2%–105.5%), a deviation of −10.7 to +9.0% (89.3%–109.0%) was obtained for shrimp. Nevertheless, it can be said that the antiBTX3 aptamer can be used successfully in BTX determination at high concentrations (>100 nM or 89.5 ng/mL).

In the SE method, considering the sensors' LOD values, 2, 100, and 1000 nM for antiBTX1; 1, 100, and 1000 nM for antiBTX2 and 100, 1000, and 2000 nM for antiBTX3 were added. For the SE method, deviations in BTX measurements added to the real samples were between −1.5 and + 3.7% (98.5%–103.7%) in fish samples for the antiBTX1 and antiBTX3 aptamers, giving a very successful result. A deviation between −6.5 and + 7.1 was obtained for shrimp, similar to TIRE (93.5%–107.1% as recovery). The antiBTX3 sensor, on the other hand, showed a deviation between −2.4 and + 7.0 in the SE configuration, providing a more successful real sample application compared to the TIRE configuration. Both methods can be reliably used for real sample (seafood) analysis, taking advantage of both aptamer selectivity and ellipsometry sensitivity.

## 4. Conclusion

In this study, two different ellipsometric transducer-based aptasensors have been developed for BTX. The analytical performance of two aptamers previously reported and another aptamer designed by excluding these aptamers were determined and compared in the BTX assay.

Ellipsometry is very sensitive to molecular deposition on the surface, especially when measured by the phase shift (Δ) in the polarization states of the reflected light. In this study, the analytical results obtained using both direct and SPR-enhanced ellipsometry were found to be comparable with the literature. It was determined that the LOD value in the SE platform, which was determined by considering only the noise level, was 39 and 129 times higher for the antiBTX1 and antiBTX2 aptamers compared to the TIRE method, respectively. Considering the interference effect, it is seen that LOD is 1.85 and 330 times higher in the SE method compared to TIRE. On average, it can be said that the LOD value obtained in the TIRE method is approximately 120 times lower than the LOD value obtained in the SE method.

However, it is interesting that the SE configuration's analytical performance in terms of sensitivity (slope of the calibration curve) was higher than TIRE in this study. With the advantage of SPR, a higher signal was received in the TIRE configuration, while the measurement's noise level has increased at a similar rate. For this reason, TIRE performance, which provides at least 10 times lower LOD and LOQ value in other studies compared to SE, this time presented an analytical performance close to SE. But, LOD values in the buffer solution in both aptamer and configurations have been quite promising (as low as 6.3 pg/mL). However, the selectivity of aptamers remained somewhat poor, especially at high concentrations of interfering compounds. Significantly, OA's structural similarity to BTX caused significant interference when compared with STX and NEO, affecting sensor analytical performances. Considering the interferent molecule signal, the best LOD values obtained for the SE system were 1.48 nM (1.32 ng/mL) for antiBTX1, and the LOD value was 0.80 nM (0.72 ng/mL) with the antiBTX1 aptamer for the TIRE configuration.

AntiBTX3, the other aptamer designed entirely by calculations on the "mfold web server", provided 0.82 nM LOD from the buffer solution at the noise level. But, since OA's interference is very high, it provided 143 nM (128 ng/mL) in SE configuration and 1.14 μM (1 μg/mL) LOD in TIRE configuration. On the other hand, the antiBTX3 aptamer in the SE configuration still provides a BTX detection limit comparable to the LC-tandem MS configuration (Table 1). Consequently, the proposed ellipsometric-based aptasensors have provided promising results in real samples for BTX detection.

## Credit author statement

**Mustafa Oguzhan Caglayan**: Conceptualization, Investigation, Methodology, Writing – original draft, Funding acquisition, Project administration. **Zafer Üstündağ**: Writing – original draft, Supervision. **Samet Şahin**: Conceptualization, Writing – review & editing, Funding acquisition

## Declaration of competing interest

The authors declare that they have no known competing financial interests or personal relationships that could have appeared to influence the work reported in this paper.

## Acknowledgments

This work was financially supported by the Scientific and Technological Research Council of Turkey (TÜBİTAK) under Grant No: 119Z191. Authors appreciate and gratefully acknowledge this financial support.

## Appendix A. Supplementary data

Supplementary data to this article can be found online at https://doi.org/10.1016/j.talanta.2021.122897.

## References

[1] S. Eissa, M. Siaj, M. Zourob, Aptamer-based competitive electrochemical biosensor for brevetoxin-2, Biosens. Bioelectron. 69 (2015) 148–154.
[2] J.S. Walker, D.J. Shaver, B.A. Stacy, L.J. Flewelling, M.H. Broadwater, Z. Wang, Brevetoxin exposure in sea turtles in south Texas (USA) during Karenia brevis red tide, Dis. Aquat. Org. 127 (2) (2018) 145–150.
[3] G.M. Hallegraeff, A review of harmful algal blooms and their apparent global increase, Phycologia 32 (2) (1993) 79–99.
[4] L.D. Mee, M. Espinosa, G. Diaz, Paralytic shellfish poisoning with a Gymnodinium catenatum red tide on the Pacific Coast of Mexico, Mar. Environ. Res. 19 (1) (1986) 77–92.
[5] T. Neely, L. Campbell, A modified assay to determine hemolytic toxin variability among Karenia clones isolated from the Gulf of Mexico, Harmful Algae 5 (5) (2006) 592–598.
[6] B. Kirkpatrick, L.E. Fleming, D. Squicciarini, L.C. Backer, R. Clark, W. Abraham, J. Benson, Y.S. Cheng, D. Johnson, R. Pierce, J. Zaias, G.D. Bossart, D.G. Baden, Literature review of Florida red tide: implications for human health effects, Harmful Algae 3 (2) (2004) 99–115.
[7] D.G. Baden, C.R. Tomas, Variations in major toxin composition for six clones of Ptychodiscus brevis, Toxicon : Off. J. Int. Soc. Toxinol. 26 (10) (1988) 961–963.

[8] R.H. Pierce, M.S. Henry, Harmful algal toxins of the Florida red tide (Karenia brevis): natural chemical stressors in South Florida coastal ecosystems, Ecotoxicology 17 (7) (2008) 623–631.
[9] K. Campbell, D.F.K. Rawn, B. Niedzwiadek, C.T. Elliott, Paralytic shellfish poisoning (PSP) toxin binders for optical biosensor technology: problems and possibilities for the future: a review, Food additives & contaminants, Part A, Chem. Anal. Contr. Exposure Risk Assess. 28 (6) (2011) 711–725.
[10] J.R. Deeds, J.H. Landsberg, S.M. Etheridge, G.C. Pitcher, S.W. Longan, Non-traditional vectors for paralytic shellfish poisoning, Mar. Drugs 6 (2) (2008) 308–348.
[11] A. Gerssen, P.P.J. Mulder, J. de Boer, Screening of lipophilic marine toxins in shellfish and algae: development of a library using liquid chromatography coupled to orbitrap mass spectrometry, Anal. Chim. Acta 685 (2) (2011) 176–185.
[12] A. Rúbies, E. Muñoz, D. Gibert, N. Cortés-Francisco, M. Granados, J. Caixach, F. Centrich, New method for the analysis of lipophilic marine biotoxins in fresh and canned bivalves by liquid chromatography coupled to high resolution mass spectrometry: a quick, easy, cheap, efficient, rugged, safe approach, J. Chromatogr. A 1386 (2015) 62–73.
[13] S.M. Etheridge, Paralytic shellfish poisoning: seafood safety and human health perspectives, Toxicon 56 (2) (2010) 108–122.
[14] S. Cestèle, W.A. Catterall, Molecular mechanisms of neurotoxin action on voltage-gated sodium channels, Biochimie 82 (9) (2000) 883–892.
[15] H.J. van den Top, C.T. Elliott, S.A. Haughey, N. Vilarino, H.P. van Egmond, L. M. Botana, K. Campbell, Surface plasmon resonance biosensor screening method for paralytic shellfish poisoning toxins: a pilot interlaboratory study, Anal. Chem. 83 (11) (2011) 4206–4213.
[16] D.G. Baden, A.J. Bourdelais, H. Jacocks, S. Michelliza, J. Naar, Natural and derivative brevetoxins: historical background, multiplicity, and effects, Environ. Health Perspect. 113 (5) (2005) 621–625.
[17] L.J. Flewelling, J.P. Naar, J.P. Abbott, D.G. Baden, N.B. Barros, G.D. Bossart, M. Y. Bottein, D.G. Hammond, E.M. Haubold, C.A. Heil, M.S. Henry, H.M. Jacocks, T. A. Leighfield, R.H. Pierce, T.D. Pitchford, S.A. Rommel, P.S. Scott, K.A. Steidinger, E.W. Truby, F.M. Van Dolah, J.H. Landsberg, Brevetoxicosis: red tides and marine mammal mortalities, Nature 435 (7043) (2005) 755–756.
[18] S.E. Fire, L.J. Flewelling, Z. Wang, J. Naar, M.S. Henry, R.H. Pierce, R.S. Wells, Florida red tide and brevetoxins: Association and exposure in live resident bottlenose dolphins (Tursiops truncatus) in the eastern Gulf of Mexico, U.S.A, Mar. Mamm. Sci. 24 (4) (2008) 831–844.
[19] D.G. Baden, V.M. Schet, K.S. Rein, R.A. Edwards, Methods for detecting brevetoxins in seawater, in biological matrices, and on excitable membranes, Bull. Soc. Pathol. Exot. 85 (5 Pt 2) (1990) 516–518, 1992.
[20] M. Campàs, B. Prieto-Simón, J.-L. Marty, Biosensors to detect marine toxins: Assessing seafood safety, Talanta 72 (3) (2007) 884–895.
[21] A. Domenech, N. Cortes-Francisco, O. Palacios, J.M. Franco, P. Riobo, J.J. Llerena, S. Vichi, J. Caixach, Determination of lipophilic marine toxins in mussels. Quantification and confirmation criteria using high resolution mass spectrometry, J. Chromatogr. A 1328 (2014) 16–25.
[22] M.W. Cao, L. Feng, P.P. Yang, H.X. Wang, X. Liang, X.W. Chen, Fabrication of reduced graphene oxide decorated with gold and nickel for the catalytic reduction of 4-nitrophenol, J. Mater. Sci. 53 (7) (2018) 4874–4883.
[23] J.F. Lawrence, B. Niedzwiadek, C. Menard, Quantitative determination of paralytic shellfish poisoning toxins in shellfish using prechromatographic oxidation and liquid chromatography with fluorescence detection: collaborative study, J. AOAC Int. 88 (6) (2005) 1714–1732.
[24] M. Okumura, H. Tsuzuki, B. Tomita, A rapid detection method for paralytic shellfish poisoning toxins by cell bioassay, Toxicon 46 (1) (2005) 93–98.
[25] Q. Wang, J. Fang, D. Cao, H. Li, K. Su, N. Hu, P. Wang, An improved functional assay for rapid detection of marine toxins, saxitoxin and brevetoxin using a portable cardiomyocyte-based potential biosensor, Biosens. Bioelectron. 72 (2015) 10–17.
[26] N.V. Kulagina, C.M. Mikulski, S. Gray, W. Ma, G.J. Doucette, J.S. Ramsdell, J. J. Pancrazio, Detection of marine toxins, brevetoxin-3 and saxitoxin, in seawater using neuronal networks, Environ. Sci. Technol. 40 (2) (2006) 578–583.
[27] Q. Wang, K. Su, L. Hu, L. Zou, T. Wang, L. Zhuang, N. Hu, P. Wang, A novel and functional assay for pharmacological effects of marine toxins, saxitoxin and tetrodotoxin by cardiomyocyte-based impedance biosensor, Sensor. Actuator. B Chem. 209 (2015) 828–837.
[28] L. Zou, C. Wu, Q. Wang, J. Zhou, K. Su, H. Li, N. Hu, P. Wang, An improved sensitive assay for the detection of PSP toxins with neuroblastoma cell-based impedance biosensor, Biosens. Bioelectron. 67 (2015) 458–464.
[29] F.M. Van Dolah, S.E. Fire, T.A. Leighfield, C.M. Mikulski, G.J. Doucette, Determination of paralytic shellfish toxins in shellfish by receptor binding assay: collaborative study, J. AOAC Int. 95 (3) (2012) 795–812.
[30] A.D. Turner, R.G. Hatfield, M. Rapkova, W. Higman, M. Algoet, B.A. Suarez-Isla, M. Cordova, C. Caceres, J. van de Riet, R. Gibbs, K. Thomas, M. Quilliam, D. N. Lees, Comparison of AOAC 2005.06 LC official method with other methodologies for the quantitation of paralytic shellfish poisoning toxins in UK shellfish species, Anal. Bioanal. Chem. 399 (3) (2011) 1257–1270.
[31] M.C. Louzao, M. Rodriguez Vieytes, A. Garcia Cabado, J.M. Vieites Baptista de Sousa, L.M. Botana, A fluorimetric microplate assay for detection and quantitation of toxins causing paralytic shellfish poisoning, Chem. Res. Toxicol. 16 (4) (2003) 433–438.
[32] P. Kele, J. Orbulescu, T.L. Calhoun, R.E. Gawley, R.M. Leblanc, Coumaryl crown ether based chemosensors: selective detection of saxitoxin in the presence of sodium and potassium ions, Tetrahedron Lett. 43 (25) (2002) 4413–4416.
[33] R.E. Gawley, H. Mao, M.M. Haque, J.B. Thorne, J.S. Pharr, Visible fluorescence chemosensor for saxitoxin, J. Org. Chem. 72 (6) (2007) 2187–2191.
[34] E. Garet, Á. González-Fernández, J. Lago, J.M. Vieites, A.G. Cabado, Comparative Evaluation of Enzyme-Linked Immunoassay and Reference Methods for the Detection of Shellfish Hydrophilic Toxins in Several Presentations of Seafood, J. Agric. Food Chem. 58 (3) (2010) 1410–1415.
[35] F.S. Chu, T.S. Fan, Indirect enzyme-linked immunosorbent assay for saxitoxin in shellfish, J. Assoc. Off. Anal. Chem. 68 (1) (1985) 13–16.
[36] R.M. Carter, M.A. Poli, M. Pesavento, D.E.T. Sibley, G.J. Lubrano, G.G. Guilbault, Immunoelectrochemical Biosensors for Detection of Saxitoxin and Brevetoxin, Immunomethods 3 (2) (1993) 128–133.
[37] S. Bratakou, G.-P. Nikoleli, C.G. Siontorou, D.P. Nikolelis, S. Karapetis, N. Tzamtzis, Development of an Electrochemical Biosensor for the Rapid Detection of Saxitoxin Based on Air Stable Lipid Films with Incorporated Anti-STX Using Graphene Electrodes, Electroanalysis 29 (4) (2017) 990–997.
[38] K. Campbell, L.D. Stewart, G.J. Doucette, T.L. Fodey, S.A. Haughey, N. Vilarino, K. Kawatsu, C.T. Elliott, Assessment of specific binding proteins suitable for the detection of paralytic shellfish poisons using optical biosensor technology, Anal. Chem. 79 (15) (2007) 5906–5914.
[39] E.S. Fonfria, N. Vilarino, K. Campbell, C. Elliott, S.A. Haughey, B. Ben-Gigirey, J. M. Vieites, K. Kawatsu, L.M. Botana, Paralytic shellfish poisoning detection by surface plasmon resonance-based biosensors in shellfish matrixes, Anal. Chem. 79 (16) (2007) 6303–6311.
[40] P. Banerjee, S. Kintzios, B. Prabhakarpandian, Biotoxin detection using cell-based sensors, Toxins (Basel) 5 (12) (2013) 2366–2383.
[41] J.J. Dorantes-Aranda, K. Campbell, A. Bradbury, C.T. Elliott, D.T. Harwood, S. A. Murray, S.C. Ugalde, K. Wilson, M. Burgoyne, G.M. Hallegraeff, Comparative performance of four immunological test kits for the detection of Paralytic Shellfish Toxins in Tasmanian shellfish, Toxicon 125 (2017) 110–119.
[42] Y. Hua, W. Lu, R.B. Cole, M.S. Henry, R.H. Pierce, On-Line High-Performance Liquid Chromatography-Electrospray Ionization Mass Spectrometry for the Determination of Brevetoxins in “Red Tide” Algae, Anal. Chem. 67 (11) (1995) 1815–1823.
[43] W. Wang, R.B. Cole, Enhanced Collision-Induced Decomposition Efficiency and Unraveling of Fragmentation Pathways for Anionic Adducts of Brevetoxins in Negative Ion Electrospray Mass Spectrometry, Anal. Chem. 81 (21) (2009) 8826–8838.
[44] J. Naar, A. Bourdelais, C. Tomas, J. Kubanek, P.L. Whitney, L. Flewelling, J. L. Karen Steidinger, D.G. Baden, A competitive ELISA to detect brevetoxins from Karenia brevis (formerly Gymnodinium breve) in seawater, shelfish, and mamalian body fluid, Environ. Health Perspect. 110 (2) (2002) 179–185.
[45] Y. Zhou, Y.S. Li, F.G. Pan, Y.Y. Zhang, S.Y. Lu, H.L. Ren, Z.H. Li, Z.S. Liu, J. H. Zhang, Development of a new monoclonal antibody based direct competitive enzyme-linked immunosorbent assay for detection of brevetoxins in food samples, Food Chem. 118 (2) (2010) 467–471.
[46] M.A. Poli, Laboratory procedures for detoxification of equipment and waste contaminated with brevetoxins PbTx-2 and PbTx-3, J. Assoc. Off. Anal. Chem. 71 (5) (1988) 1000–1002.
[47] M.A. Poli, V.R. Rivera, D.D. Neal, D.G. Baden, S.A. Messer, S.M. Plakas, R. W. Dickey, K.E. Said, L. Flewelling, D. Green, J. White, An electrochemiluminescence-based competitive displacement immunoassay for the type-2 brevetoxins in oyster extracts, J. AOAC Int. 90 (1) (2007) 173–178.
[48] S.M. Plakas, R.W. Dickey, Advances in monitoring and toxicity assessment of brevetoxins in molluscan shellfish, Toxicon : Off. J. Int. Soc. Toxinol. 56 (2) (2010) 137–149.
[49] Y. Tang, Z. Ali, J. Zou, G. Jin, J. Zhu, J. Yang, J. Dai, Detection methods for Pseudomonas aeruginosa: history and future perspective, RSC Adv. 7 (82) (2017) 51789–51800.
[50] J. Tang, L. Hou, D. Tang, J. Zhou, Z. Wang, J. Li, G. Chen, Magneto-controlled electrochemical immunoassay of brevetoxin B in seafood based on guanine-functionalized graphene nanoribbons, Biosens. Bioelectron. 38 (1) (2012) 86–93.
[51] D. Tang, B. Zhang, J. Tang, L. Hou, G. Chen, Displacement-type quartz crystal microbalance immunosensing platform for ultrasensitive monitoring of small molecular toxins, Anal. Chem. 85 (14) (2013) 6958–6966.
[52] D. Tang, J. Tang, B. Su, G. Chen, Gold nanoparticles-decorated amine-terminated poly(amidoamine) dendrimer for sensitive electrochemical immunoassay of brevetoxins in food samples, Biosens. Bioelectron. 26 (5) (2011) 2090–2096.
[53] S.M. Handy, B.J. Yakes, J.A. DeGrasse, K. Campbell, C.T. Elliott, K.M. Kanyuck, S. L. Degrasse, First report of the use of a saxitoxin-protein conjugate to develop a DNA aptamer to a small molecule toxin, Toxicon 61 (2013) 30–37.
[54] P. Hu, Z. Liu, R. Tian, H. Ren, X. Wang, C. Lin, S. Gong, X. Meng, G. Wang, Y. Zhou, S. Lu, Selection and identification of a DNA aptamer that mimics saxitoxin in antibody binding, J. Agric. Food Chem. 61 (14) (2013) 3533–3541.
[55] A.D. Ellington, J.W. Szostak, In vitro selection of RNA molecules that bind specific ligands, Nature 346 (6287) (1990) 818–822.
[56] C. Tuerk, L. Gold, Systematic evolution of ligands by exponential enrichment: RNA ligands to bacteriophage T4 DNA polymerase, Science (New York, N.Y.) 249 (4968) (1990) 505–510.
[57] K.M. Song, S. Lee, C. Ban, Aptamers and their biological applications, Sensors 12 (1) (2012) 612–631.
[58] I. Cunha, R. Biltes, M. Sales, V. Vasconcelos, Aptamer-Based Biosensors to Detect Aquatic Phycotoxins and Cyanotoxins, Sensors (Basel) 18 (7) (2018) 2367.
[59] H. Wu, M. Guo, Z. Tan, H. Cheng, Z. Li, Y. Zhai, Liquid chromatography quadrupole linear ion trap mass spectrometry for multiclass screening and identification of lipophilic marine biotoxins in bivalve mollusks, J. Chromatogr. A 1358 (2014) 172–180.

[60] M.P. Kreuzer, M. Pravda, C.K. O'Sullivan, G.G. Guilbault, Novel electrochemical immunosensors for seafood toxin analysis, Toxicon : Off. J. Int. Soc. Toxinol. 40 (9) (2002) 1267–1274.
[61] M. Poksinski, H. Arwin, Protein monolayers monitored by internal reflection ellipsometry, Thin Solid Films 455–456 (2004) 716–721.
[62] K. Campbell, D.F. Rawn, B. Niedzwiadek, C.T. Elliott, Paralytic shellfish poisoning (PSP) toxin binders for optical biosensor technology: problems and possibilities for the future: a review, Food Addit. Contam. Part A Chem Anal Control Expo Risk Assess 28 (6) (2011) 711–725.
[63] S.A. Haughey, K. Campbell, B.J. Yakes, S.M. Prezioso, S.L. Degrasse, K. Kawatsu, C. T. Elliott, Comparison of biosensor platforms for surface plasmon resonance based detection of paralytic shellfish toxins, Talanta 85 (1) (2011) 519–526.
[64] Z. Üstündağ, M.O. Çağlayan, R. Güzel, E. Pişkin, A.O. Solak, A novel surface plasmon resonance enhanced total internal reflection ellipsometric application: electrochemically grafted isophthalic acid nanofilm on gold surface, Analyst 136 (7) (2011) 1464–1471.
[65] M.O. Caglayan, Z. Üstündağ, Spectrophotometric ellipsometry based Tat-protein RNA-aptasensor for HIV-1 diagnosis, Spectrochim. Acta Mol. Biomol. Spectrosc. 227 (2020) 117748.
[66] M.O. Caglayan, Z. Üstündağ, Detection of zearalenone in an aptamer assay using attenuated internal reflection ellipsometry and it's cereal sample applications, Food Chem. Toxicol. 136 (2020) 111081.
[67] M.O. Caglayan, Z. Üstündağ, Saxitoxin aptasensor based on attenuated internal reflection ellipsometry for seafood, Toxicon: Off. J. Int. Soc. Toxinol. 187 (2020) 255–261.
[68] M.O. Çağlayan, F. Sayar, G. Demirel, B. Garipcan, B. Otman, B. Çelen, E. Pişkin, Stepwise formation approach to improve ellipsometric biosensor response, Nanomed. Nanotechnol. Biol. Med. 5 (2) (2009) 152–161.
[69] M.O. Caglayan, Mercuric ion detection by plasmon-enhanced spectrophotometric ellipsometer using specific oligonucleotide probes, Spectrochim. Acta Mol. Biomol. Spectrosc. 241 (2020) 118682.
[70] M.O. Caglayan, Aptamer-based ellipsometric sensor for ultrasensitive determination of aminoglycoside group antibiotics from dairy products, J. Sci. Food Agric. 100 (8) (2020) 3386–3393.
[71] M.O. Caglayan, Plasmon resonance-enhanced internal reflection ellipsometry for the trace detection of mercuric ion, Int. J. Environ. Sci. Technol. 15 (4) (2018) 909–914.
[72] E. Kretschmann, H. Raether, Notizen: Radiative Decay of Non Radiative Surface Plasmons Excited by Light, Z. Naturforsch. 23 (12) (1968) 2135.
[73] M.O. Caglayan, Z. Ustundag, Saxitoxin aptasensor based on attenuated internal reflection ellipsometry for seafood, Toxicon : Off. J. Int. Soc. Toxinol. 187 (2020) 255–261.
[74] E.P. Pinto, S.M. Rodrigues, N. Gouveia, V. Timóteo, P.R. Costa, Tetrodotoxin and saxitoxin in two native species of puffer fish, Sphoeroides marmoratus and Lagocephalus lagocephalus, from NE Atlantic Ocean (Madeira Island, Portugal), Mar. Environ. Res. 151 (2019) 104780.
[75] I. Russo Krauss, A. Pica, A. Merlino, L. Mazzarella, F. Sica, Duplex-quadruplex motifs in a peculiar structural organization cooperatively contribute to thrombin binding of a DNA aptamer, Acta crystallographica, Sec. D, Biol. Crystallogr. 69 (Pt 12) (2013) 2403–2411.
[76] A. Afanasyeva, C. Nagao, K. Mizuguchi, Prediction of the secondary structure of short DNA aptamers, Biophys. Physicobiol. 16 (2019) 287–294.
[77] S.C.B. Gopinath, T. Lakshmipriya, M.K. Md Arshad, C.H. Voon, T. Adam, U. Hashim, H. Singh, S.V. Chinni, Shortening full-length aptamer by crawling base deletion – Assisted by Mfold web server application, J. Assoc. Arab Univ. Basic Appl. Sci. 23 (2017) 37–42.
[78] X. Zheng, B. Hu, S.X. Gao, D.J. Liu, M.J. Sun, B.H. Jiao, L.H. Wang, A saxitoxin-binding aptamer with higher affinity and inhibitory activity optimized by rational site-directed mutagenesis and truncation, Toxicon: Off. J. Int. Soc. Toxinol. 101 (2015) 41–47.